IEEE Access
Multidisciplinary ⋮ Rapid Review ⋮ Open Access Journal

Received 13 January 2024, accepted 23 January 2024, date of publication 30 January 2024, date of current version 5 February 2024.

Digital Object Identifier 10.1109/ACCESS.2024.3358677

RESEARCH ARTICLE

A New Class of High-Selectivity Bandpass Filters With Constant Bandwidth and 5:1 Bandwidth Tuning Ratio

PHOTOS VRYONIDES[1,2], (Senior Member, IEEE), SALMAN ARAIN[3], (Member, IEEE), ABDUL QUDDIOUS[4], (Member, IEEE), DIMITRA PSYCHOGIOU[5,6], (Senior Member, IEEE), AND SYMEON NIKOLAOU[1,2], (Senior Member, IEEE)

[1]Department of Electrical and Computer Engineering and Informatics, Frederick University, 1036 Nicosia, Cyprus
[2]Frederick Research Center (FRC), 1036 Nicosia, Cyprus
[3]Electrical Engineering Department, NFC Institute of Engineering and Fertilizer Research, Faisalabad 38000, Pakistan
[4]Chair for RF and Photonics Engineering, Technische Universität Dresden, 01187 Dresden, Germany
[5]School of Engineering, University College Cork, Cork 021, T12 K8AF Ireland
[6]Tyndall National Institute, Cork 021, T12 R5CP Ireland

Corresponding author: Dimitra Psychogiou (dpsychogiou@ucc.ie)

This work was partially co-funded by the Republic of Cyprus, through the EXCELLENCE/0421/0495 (SMURFS) project which is implemented under the Cohesion Policy Funds "THALEIA 2021-2027" with EU co-funding, and by the ENTERPRISES/0223/Sub-Call1/276 ROMANIA project co-funded by the Recovery and Resilience Facility of the Next Generation EU instrument.

ABSTRACT This paper presents a design for compact bandpass filters (BPFs) that feature high selectivity. This high selectivity is achieved through the use of open-/short-circuited coupled-line segments at the filter's input and output and a pair of symmetrical parallel-coupled lines connected to a pair of open stepped-impedance resonators (SIRs) introducing three transmission zeros (TZs) on either side of the passband. In addition, two different designs for these BPFs, one with a fixed bandwidth and one with a tunable bandwidth are also presented. The characteristics of the proposed structure are analyzed using even-, odd-mode and ABCD analyses. To enable bandwidth tuning, two varactor diodes are added to the edges of the open SIRs, allowing the TZs to be adjusted around the upper band edge. The paper includes details of two prototypes that were designed, fabricated, and tested: Filter A with a constant bandwidth that covers the entire S-band (2-4 GHz) and a 3-dB fractional bandwidth (FBW) of 60%, and Filter B with a tunable bandwidth and a 3-dB FBW that varies from 12% to 60%. The filters have been measured to have insertion loss of less than 0.8 dB for Filter A and less than 1.1 dB for Filter B throughout the passband, and return loss of greater than 16 dB and 15 dB for Filter A and B, respectively. These filters have a compact size of less than $0.113\lambda_g^2$, and feature high selectivity with a wide 3-dB bandwidth tuning range ratio, as well as an upper stopband suppression level of more than 40 dB.

INDEX TERMS Bandpass filter (BPF), parallel-coupled lines, selectivity, transmission zeros (TZs).

I. INTRODUCTION

Compact planar microwave passive bandpass filters (BPFs) with superior selectivity and high-performance characteristics such as passband flatness, low insertion loss, sharp roll-off skirt, and high out-of-band rejection are some of the main filter performance requirements for modern RF communication systems. A variety of design approaches and structures has been published in literatures [1], [2], [3], [4], [5], [6], [7], [8], [9], [10], [11], and [12]. In particular, [1] reports the implementation of different pairs of coupled lines in a BPF with multiple transmission zeros (TZs) and transmission poles (TPs). In [2], a new technique for designing a high-selectivity filter using a coupled-line structure is proposed, with the downside of only adding one pair of symmetrical TZs. In addition, [3] describes a BPF with compact size

The associate editor coordinating the review of this manuscript and approving it for publication was Giorgio Montisci.

and two pairs of TZs that uses coupled lines and open/shorted stubs. Pairs of coupled lines are also reported in [4] to improve the out-of-band interference and roll-off rates (ROR). Even though it is only valid for dual- band filters, [5] proposes a new method to enhance the selectivity by adding two open-circuited sections to the input and output stages. Reference [6] introduces transversal signal-interaction principles to illustrate a new approach for developing BPFs with superior selectivity with many TZs. To achieve a large stopband interference at the cost of weak in-band selectivity, open stubs are linked to the input/output stages in [7], and in [8] the upper stopband rejection is improved by using shunt-shorted stubs. A new method to achieve a wide stopband with high selectivity using cross-coupled spur lines is proposed in [9] whereas in [10] high selectivity with controllable transmission zeros is achieved using substrate integrated waveguide (SIW) technology. Recently, in order to minimize the cross talk while preserving high stop band rejection and low insertion loss low-temperature co-fired ceramic (LTCC) based BPFs [11], [12] were proposed using stepped impedance resonators (SIRs) and quasi-lumped and distributed elements respectively. Due to the endless need for small-sized and low-power transceivers, the use of a single agile device is preferred over using multiple devices. Earlier works mainly concern BPFs with center frequency agility in [13], [14], [15], [16], and [17] and switchable bandwidths [18], [19], [20], [21]. However, fewer efforts have been dedicated to the design of tunable bandwidth BPFs [22], [23], [24]. In [25], bandwidth tunability is achieved by independently controlling the adjustable TZs. Good performances have been reported with filters using a cross-shaped resonator, a T-shaped resonator, and a higher order coaxial-based resonator [26], [27], [28], [29] or with filters based on short sections of parallel coupled lines and short-circuited stub resonators [30], [31], [32], [33], [34], [35].

This paper demonstrates a new method for designing a high-selectivity BPF with six finite TZs that covers the S-band frequency spectrum while maintaining a compact size. It uses two open/short-circuited coupled lines (OSCLs) at the filter's input and output ports. The circuit also includes symmetrical parallel coupled-lines (PCLs) and open-stepped impedance resonators (SIRs) at the symmetry plane. Two varactor diodes are placed at the open SIR edges to adjust the bandwidth. Varactor capacitances can tune the top band edge while keeping the lower band edge unchanged. This research work makes a significant contribution in the field of compact bandpass filters (BPFs) by introducing a novel technique to generate two pairs of additional transmission zeros (TZs) on the left and right sides of the passband region. This is achieved by using $\lambda_g/2$ open- and short-circuited coupled lines at the input and output ports. This work for the first time introduces a new technique to generate two pairs of additional TZs on the left and right sides of the passband region. This approach allows for the creation of symmetric pairs of TZs, while maintaining the compact size of the BPF. Additionally, this technique can be applied to a tunable BPF design.

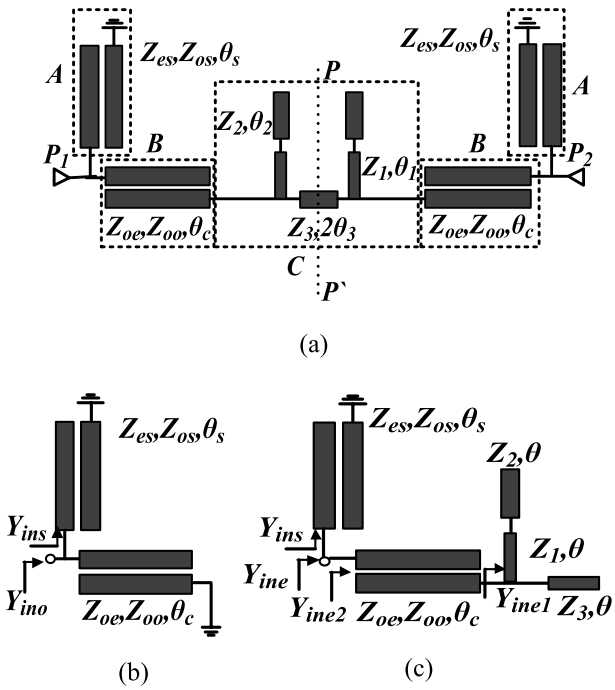

FIGURE 1. Design configuration and even-odd mode equivalent circuits. (a) Geometrical configuration of BPF, (b) Odd-mode, (c) Even-mode.

The remaining part of this paper is outlined as follows. The proposed filter's analysis is presented in Section II, followed by the tunable bandwidth BPF's analysis in Section III. Section IV presents two filter prototypes based at 3 GHz that designed and tested for validation purposes. Finally, a discussion and the main contributions of this work are provided in Section V.

II. THEORY AND DESIGN EQUATIONS FOR FILTERS

A. TRANSMISSION POLES AND ZEROS

The geometrical configuration of the proposed BPF is shown in Fig. 1(a). It consists of two $\lambda_g/2$ long open-/short- circuited coupled- lines (OSCLs) that are connected to the input and output ports represented by Z_{es}, Z_{os} and electrical length θ_s and a uniform transmission line with two stepped-impedance stubs (resonator) denoted by Z_1, θ_1 and Z_2, θ_2. A pair of $\lambda_g/4$ long symmetrical PCLs with an electrical length of θ_c serves as the main transmission line. The PCLs' even-mode and odd-mode impedances are Z_{oe} and Z_{oo}, respectively.

The open circuited SIRs are separated by a transmission line with constant width, characteristic impedance Z_3, and electrical length $2\theta_3$. Due to the symmetrical configuration, the even- and odd-mode methods can be used to investigate the resonator's operation on the symmetry plane PP'. The voltage zero is applied in the middle of the main transmission line in odd-mode excitation. The odd-mode equivalent circuit is shown in Fig. 1. (b). The symmetrical plane PP' can be modelled as a complete magnetic-wall in even mode excitation, as seen in the analogous circuit of Fig. 1(c). Notably, the inclusion of OSCLs, each of a length equal to $\lambda_g/2$, not

only enhances coupling but also leads to the generation of additional transmission zeros. When $Y_{ine} = 0$, the even mode resonant frequencies can be computed by ignoring the folded junction discontinuity and assuming $\theta_1 = \theta_2 = \theta_3$ to simplify mathematical calculations:

$$Y_{ine1} = j\frac{(Z_1 + Z_2)A\ tan\ \theta}{Z_1(Z_2 - Z_1\ tan^2\theta)} + \frac{j\ tan\ \theta}{Z_3} \tag{1}$$

$$Y_{ine2} = \frac{\frac{4}{Y_{ine1}} + j2C\ cot\ \theta_c}{C\left(\frac{-j2\ cot\ \theta_c}{Y_{ine1}} + cot^2\ \theta_c - E^2\csc^2\theta_c\right)} \tag{2}$$

$$Y_{ins} = -j\frac{A\ sin\ 2\theta_s}{A\ sin^2\ \theta_s - 4B} \tag{3}$$

$$Y_{ine} = Y_{ins} + Y_{ine2} \tag{4}$$

To find the even mode resonances $Y_{ine} = 0$

$$Y_{ine} = (4A^2 + 4AE)\ sin^4\theta_c - (4A^2 + 6AE)\ sin^2\theta_c + (2AE + 4B) = 0 \tag{5}$$

Similarly, by setting $Y_{ino} = 0$ and using the assumption that $\theta_s = 2\theta_c$, the odd-mode resonant frequencies can be calculated using equation (6).

$$Y_{ino} = (2AC^2 + 2A^2C)\ sin^4\theta_c - (2A^2C + AC^2 + 8AD)\ sin^2\theta_c + (4AD + 2BC) = 0 \tag{6}$$

Similarly, the even- and odd-mode poles can be calculated using the following equation (7) and equation (8), as shown at the bottom of the next page, where, $A = Z_{es} + Z_{oo}$, $B = Z_{es}Z_{os}$, $C = Z_{oe} + Z_{oo}$ and $D = Z_{oe}Z_{oo}E = Z_{oe} + Z_{oo}$

Furthermore, by transforming the ABCD matrix into a Y_T matrix, the TZs of the structure shown in Fig. 1(a) can be calculated. The ABCD matrix is extracted from Fig. 1(a) and given in (9) as:

$$[ABCD]_T = [ABCD]_A \times [ABCD]_B \times [ABCD]_C \times [ABCD]_B \times [ABCD]_A \tag{9}$$

where,

$$[ABCD]_A = \begin{bmatrix} A_1 & A_2 \\ A_3 & A_4 \end{bmatrix} \tag{10}$$

$$[ABCD]_B = \begin{bmatrix} B_1 & B_2 \\ B_3 & B_4 \end{bmatrix} \tag{11}$$

$$[ABCD]_C = \begin{bmatrix} C_1 & C_2 \\ C_3 + C_3' & C_4 \end{bmatrix} \tag{12}$$

and the coefficient values are:

$$A_1 = \frac{Z_{es} - Z_{os}}{Z_{es} + Z_{os}}\csc^2\theta_s - \frac{Z_{es} + Z_{os}}{Z_{es} - Z_{os}}cot^2\theta_s \tag{13}$$

$$A_2 = -j\frac{2Z_{es}Z_{os}}{Z_{es} - Z_{os}}cot\theta_s \tag{14}$$

$$A_3 = -j\frac{2}{Z_{es} - Z_{os}}cot\theta_s \tag{15}$$

$$A_4 = \frac{Z_{es} + Z_{os}}{Z_{es} - Z_{os}} \tag{16}$$

$$B_1 = \frac{Z_{oe} + Z_{oo}}{Z_{oe} - Z_{oo}}\cos\theta_c \tag{17}$$

$$B_2 = j\frac{(Z_{oe} - Z_{oo})^2 - (Z_{oe} + Z_{oo})^2\cos^2\theta_c}{2(Z_{oe} - Z_{oo})\sin\theta_c} \tag{18}$$

$$B_3 = j\frac{2\sin\theta_c}{Z_{oe} - Z_{oo}} \tag{19}$$

$$B_4 = B_1 \tag{20}$$

$$C_1 = \cos 2\theta - \frac{2(Z_1Z_2Z_3)\ sin^2\theta}{Z_1Z_2 - Z_1^2 tan^2\theta} \tag{21}$$

$$C_2 = jZ_3\ sin\ 2\theta \tag{22}$$

$$C_3 = \frac{jsin2\theta}{Z_3} \tag{23}$$

$$C_3' = \frac{j\left[2(Z_1 + Z_2)\cos 2\theta tan\theta - \frac{(Z_1+Z_2)^2Z_3\ sin^2\theta tan\theta}{Z_1Z_2 - Z_1^2 tan^2\theta}\right]}{Z_1Z_2 - Z_1^2 tan^2\theta} \tag{24}$$

$$C_4 = \cos 2\theta - \frac{2(Z_1Z_2Z_3)\ sin^2\theta}{Z_1Z_2 - Z_1^2 tan^2\theta} \tag{25}$$

Y_{21} can be extracted by converting the matrix $[ABCD]_T \Rightarrow [Y]_T$ as given in (26), as shown at the bottom of the next page. The solutions obtained from (26) correspond to the constant transmission zeros of the PCLs, $f_{TZ1} = 0$ and $f_{TZ6} = 2f_c$, respectively, as well as f_{TZ2}-f_{TZ5}, which are discussed in detail in section B.

B. ANALYSIS OF THE SELECTIVITY IMPROVEMENT TECHNQIUE

This section shows how the open/short-circuited coupled lines add two pairs of symmetrical TZs through a mathematical analysis. Z_{ins} is the input impedance of the coupled line component, as shown in Fig.1 (a). When Z_{ins} is infinity or zero, it can be thought of as a two-port network having a BPF or an all-stop response [36]. The input impedance of the coupled line segment of Fig. 1(a) can be obtained as follows:

$$Z_{ins} = j\frac{(Z_{es} + Z_{os})^2\ sin^2\theta_s - 4Z_{es}Z_{os}}{(Z_{es} + Z_{os})\ sin\ 2\theta_s} \tag{27}$$

Since it is preferable to have Z_{ins} infinite at the BPF's central frequency f_c, θ_s needs to be set to π at f_c to achieve a bandpass response and two pairs of symmetrical TZs when Z_{ins} is zero.

As a result, (27) can be rewritten as,

$$Z_{ins} = j\frac{(Z_{es}+Z_{os})^2\ sin^2(\pi f/f_c) - 4Z_{es}Z_{os}}{(Z_{es}+Z_{os})\ sin\ (2\pi f/f_c)} \tag{28}$$

where f is the operating frequency. The locations of the TZs can be found if $f = f_c$ and (28) are set to zero. Then, by defining $q = Z_{os}/Z_{es}$ (28) becomes,

$$(q + 1)^2\ sin^2\theta_s - 4q = 0 \tag{29}$$

$\alpha = 2\sqrt{q}/(q + 1)$ With valid solutions θ_s at $(2n+1)\pi \pm \sin^{-1}\alpha$ and at $2n\pi \pm \sin^{-1}\alpha$ where n= 0,1,2,...and $\alpha = 2\sqrt{q}/(q + 1)$

From (29) it is derived that the OSCL section can generate two pairs of symmetrical TZs at,

$$f_{TZ2} = \frac{f_c}{\pi}\ sin^{-1}\alpha \tag{30}$$

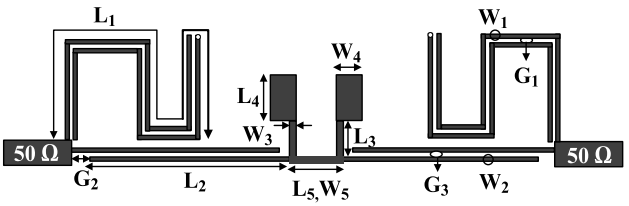

(a)

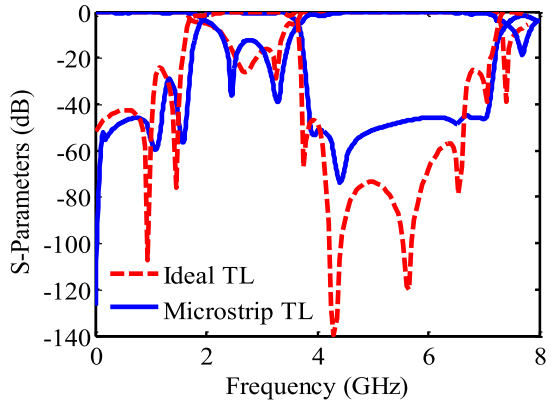

(b)

FIGURE 2. (a) Proposed BPF with enhanced selectivity, Dimensions: $W_1 = 0.45$, $W_2 = 0.20$, $W_3 = 0.70$, $W_4 = 3.20$, $W_5 = 0.65$, $L_1 = 34.0$, $L_2 = 16.90$, $L_3 = 2.90$, $L_4 = 4.45$, $L_5 = 5.76$, $G_1 = 0.45$, $G_2 = 0.30$, $G_3 = 0.37$ (all units in mm). (b). Simulated comparison between ideal and microstrip transmission line (TL) models.

$$f_{TZ3} = \frac{f_c}{\pi}\left(\pi - sin^{-1}\alpha\right) \tag{31}$$

$$f_{TZ4} = \frac{f_c}{\pi}\left(\pi + sin^{-1}\alpha\right) \tag{32}$$

$$f_{TZ5} = \frac{f_c}{\pi}\left(2\pi - sin^{-1}\alpha\right) \tag{33}$$

Since TZs' positions are determined by the impedance ratio q, valid 'q' solutions are as follows:

$$q = 2\left[\frac{1 \pm cos(\pi\rho)}{sin^2(\pi\rho)}\right] - 1 \tag{34}$$

where ρ is defined as θ_s/π.

(29) also exemplifies that the OSCL section generates two pairs of symmetrical TZs at $f_c(1\pm\rho)$, $f_c\rho$, and $f_c(2\text{-}\rho)$.

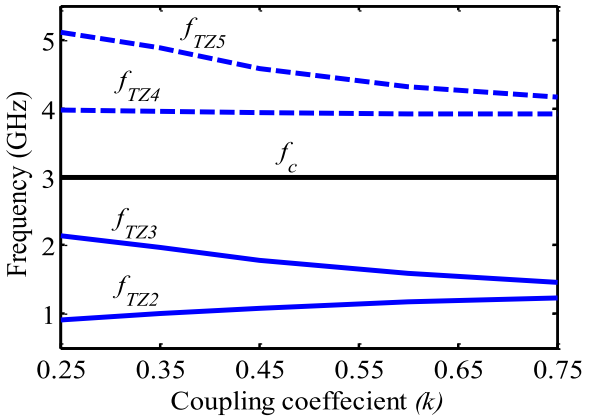

(a)

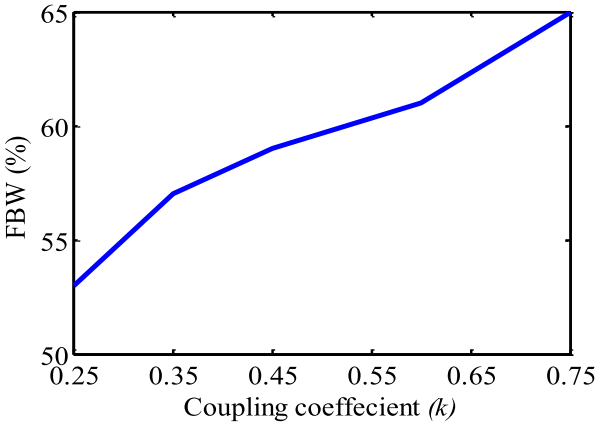

(b)

FIGURE 3. (a) Calculated TZs vs k (b) FBW vs k.

With the aim of obtaining four TZs at 1.2 GHz, 1.8 GHz, 4.2 GHz and 4.8 GHz, ρ should be set to 0.4 and by using (34), $q = 0.53$.

The geometrical layout of the proposed BPF is presented in Fig. 2(a). In Fig. 2(b), both ideal and microstrip transmission line models comparison is presented demonstrating a good agreement. As can be seen, two folded $\lambda_g/2$ open-/short-circuited coupled lines are added to both input and output of the filter. Consequently, two pairs of TZs are produced

$$f_{op} = \frac{2f_o}{\pi} sin^{-1}\left[\sqrt{\frac{(2A^2C + AC^2 + 8AD) \pm \sqrt{(2A^2C + AC^2 + 8AD)^2 - (8AC^2 + 2A^2C)(4AD + 2BC)}}{4AC^2 + 4A^2C}}\right] \tag{7}$$

$$f_{ep} = \frac{2f_o}{\pi} sin^{-1}\left[\sqrt{\frac{(4A^2 + 6AC) \pm \sqrt{(4A^2 + 6AE)^2 - (16A^2 16AE)(2AE + 4B)}}{8A^2 + 8AE}}\right] \tag{8}$$

$$Y_{21} = \frac{2j\, Z_1 Z_2 (Z_{oe} - Z_{oo})^2 \sin^2\theta_c [(Z_{es} - Z_{os})^2 - (Z_{es} + Z_{os})^2 \cos^2\theta_s]}{(Z_{es} - Z_{os})(Z_{es} + Z_{os}) \sin^2\theta_s [(Z_{oe} + Z_{oo})^2 \cos^2\theta_c - (Z_{oe} - Z_{oo})^2][2Z_1 Z_2 (Z_{oe} + Z_{oo}) \cos^2\theta_c \sin\theta_c - (Z_1 + Z_2)(Z_{oe} - Z_{oo}) tan\theta_1 + (Z_1 + Z_2)(Z_{oe} + Z_{oo})^2 \cos^2\theta_c tan\theta_1]} \tag{26}$$

at both edges of the passband. Figs 3(a) and (b) show the TZs locations and 3-dB fractional bandwidth (FBW) as a function of the coupling coefficient k, where $k = (Z_{es}\text{-}Z_{os})/(Z_{es} + Z_{os})$, for $Z_{oe} = 159\ \Omega$ and $Z_{oo} = 69\ \Omega$ and fixed electrical length $\theta_c = 90°$ and $\theta_s = 180°$. Also, for the proposed design, $Z_1 = 81.40\ \Omega$, $Z_2 = 33.84\ \Omega$, $Z_3 = 84.04\ \Omega$ along with corresponding electrical lengths as $\theta_1 = 16.73°$, $\theta_2 = 27.40°$, $\theta_3 = 33.15°$. As 'k' rises, the lower band zero close to the passband's edge, f_{TZ3}, shifts to lower frequency thus increasing the FBW.

Fig. 4(a) shows $|S_{21}|$ responses of three different illustrations (whole filter, filter without coupled lines, and OSCLs only) for demonstration purposes. As demonstrated, superior selectivity in the BPF is obtained when the OSCLs are attached having a total of six TZs up to $2f_c$. Four of TZs are produced by the added $\lambda_g/2$ OSCLs and the rest by the $\lambda_g/4$ parallel-coupled lines.

III. TUNABLE BANDWIDTH

By the insertion of two varactor diodes at the edge of the two open- circuited SIRs of the design configuration of Fig.1 (a), a BPF with tunable bandwidth can be implemented. Assuming $\theta_1 = \theta_2 = \theta$ for simplicity, the ABCD matrix of the varactor loaded with open SIR stub, can be written as:

$$[ABCD]_{SIR} = \begin{bmatrix} A_{SIR} & B_{SIR} \\ C_{SIR} & D_{SIR} \end{bmatrix} = \begin{bmatrix} 1 & 0 \\ 1/Z_{in} & 1 \end{bmatrix} \tag{35}$$

where the input impedance of the open SIR with a varactor diode Z_{in} is expressed as:

$$Z_{in} = -jZ_1 \frac{Z_2 - Z_1 tan^2\theta - \omega C tan\theta(Z_2^2 + Z_1 Z_2)}{\omega C Z_1 Z_2 - \omega C Z_2^2 tan^2\theta + tan\theta(Z_1 + Z_2)} \tag{36}$$

Thus, the loaded capacitance C_v of the varactor in this tunable filter can be derived from the transmission zero frequency f_z around the upper band edge as:

$$C_v = \frac{Z_2 - Z_1 tan^2\theta}{2\pi f_z tan\theta(Z_2^2 + Z_1 Z_2)} \tag{37}$$

Fig. 4(b) shows the degree of change of the resonant frequencies and TZs for different capacitance values of the varactor, C_v. It can be deduced from the results that two transmission poles (TPs) are employed in the filter design. It is also worth noticing that C_v has no effect on f_{TZ1}, f_{TZ2} and f_{TZ3} as anticipated and has a slight effect on f_{TP1} and f_{TP2}. In addition, as C_v increases f_{TZ4} moves towards lower values. Therefore, the upper edge of the passband is independently controlled by changing C_v. A BPF with a tunable bandwidth edge can thus be implemented by using two varactor diodes and the above design method.

IV. DESIGN PROCEDURE AND EXAMPLE OF BPFs WITH CONSTANT AND TUNABLE BANDWIDTH

Following the preceding discussion, a summary of the simple design procedure for the proposed BPF with constant bandwidth (Filter A) is given as:

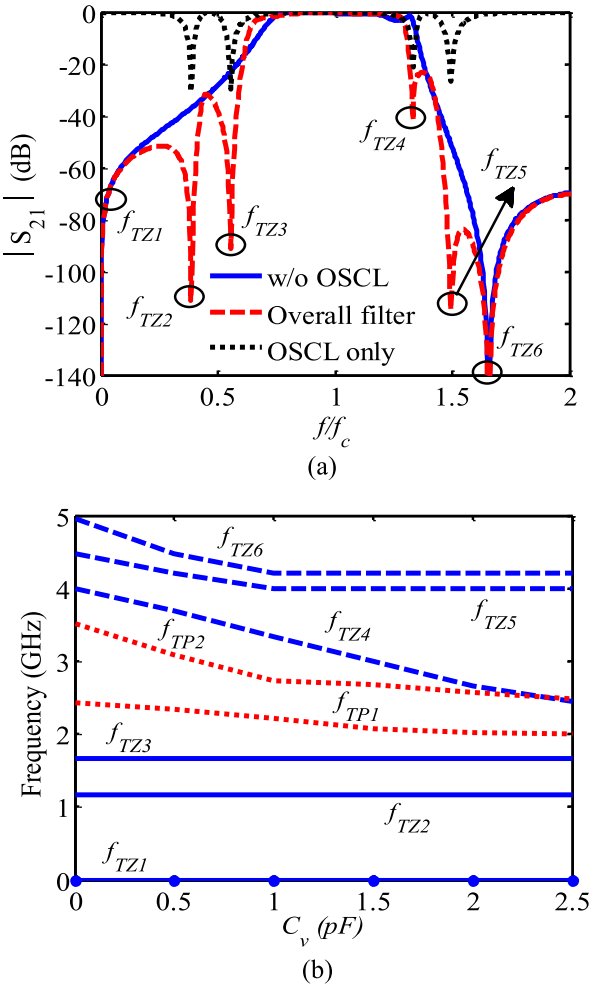

FIGURE 4. (a) Transmission $|S_{21}|$ responses of the proposed high-selectivity BPF of Fig. 2 with and without the OSCLs and $|S_{21}|$ response of OSCLs only,(b) Effects from the varactor's capacitance on TZs and TPs.

1) Choose your preferred center frequency (f_c), passband bandwidth, passband return loss, and stopband isolation.
2) Select suitable value for ρ and calculate q.
3) Select appropriate values for Z_1, Z_2, and Z_3 along with corresponding electrical lengths θ_1, θ_2, and θ_3.
4) Set L_1 and L_2 to around $\lambda_g/2$ and $\lambda_g/4$ respectively.
5) Adjust the impedance values of Z_1, Z_2, Z_{oo}, Z_{oe}, Z_{es} and Z_{os} slightly to achieve the best possible filter performance.

The design procedure for the BPF with tunable bandwidth (Filter B) can be summarized as follows:

1) Decide the specifications for the tunable BPF for the widest bandwidth state, i.e. center frequency (f_c), passband bandwidth.
2) Determine the dimensions and layout on the basis of the design procedure for the BPF with constant bandwidth.
3) Insert a pair of varactor diodes at the open SIRs edges and then optimize the dimensions. The final

TABLE 1. Comparison between calculated, simulated & measured resonant frequencies (units: GHz).

Frequencies	Calculated	Simulated	Measured
f_{TZ2}	1.20	1.18	1.10
f_{TZ3}	1.80	1.71	1.62
f_{TZ4}	4.20	4.00	4.26
f_{TZ5}	4.80	4.60	4.86

TABLE 2. Comparison with state-of-the-art BPFs.

Ref.	C.F (GHz)	TZ (GHz)	FBW (%)	IL, RL (dB)	ROR (Lower/upper) (dB/GHZ)	Upper stopband rejection (dB)	Circuit Size ($\lambda_g \times \lambda_g$)
[1]	2.05	8	60	0.6, 20	110/55	> 20 (2.8-5.2 GHz)	0.48×0.24
[3]	1.93	4	78	0.8, 15	288/175	> 35 (2.9-5.0 GHz)	0.56×0.23
[4]	2.10	8	19	1.8, 12	45/110	> 18 (2.3-5.8 GHz)	0.39×0.28
[6]	3.0	6	62	0.4, 15	210/130	> 15 (4.5-7.7 GHz)	0.68×0.53
Our work	**3.0**	6	**60**	**0.8, 13**	155/130	**> 40 (3.9-7.1GHz)**	**0.67×0.17**

dimensions are determined with the help of commercially available full wave simulation packages.

A. BPF WITH CONSTANT BANDWIDTH FILTER (FILTER A)

To validate the proposed concept a prototype was implemented on Roger 4003C substrate with $\varepsilon_r = 3.55$ and thickness $h = 0.813$ mm. The fabricated BPF prototype along with simulated and measured S- parameters are shown in Fig. 5(a) and Fig. 5(b) respectively. The simulated and measured S- parameters appear to be in good agreement, validating the design concept. The 3-dB FBW for $f_c = 3$ GHz is 60 %. An insertion loss less than 0.8 dB, and return loss of more than 16 dB were measured in the upper stopband rejection from 3.9-7.1 GHz are attained. The group delay was measured between 0.25- 0.32 ns in the passband region as shown in Fig. 5(c). The roll-off rate (ROR) is used to measure the steepness of the transition band and is defined as,

$$ROR_{20dB} = \frac{|A_{20dB} - A_{3dB}|}{|f_{20dB} - f_{3dB}|} \tag{38}$$

where A_{3dB} and A_{20dB} are the 3- and 20-dB attenuation points respectively, and f_{3dB} and f_{20dB} are the 3- and 20-dB stopband frequency points respectively.

Based on the equations, the comparison between the calculated, simulated and measured results is presented in Table 1. Table 2 shows a comparison of the proposed BPF with some other BPFs that have been published. It is indicated that the suggested BPF has six TZs with high selectivity, good upper stopband rejection performance with small size, in addition to the attractive insertion and return loss characteristics.

B. BPF WITH TUNABLE BANDWIDTH (FILTER B)

The final dimensions and layout for the tunable bandwidth filter are determined with the aid of the design procedure for

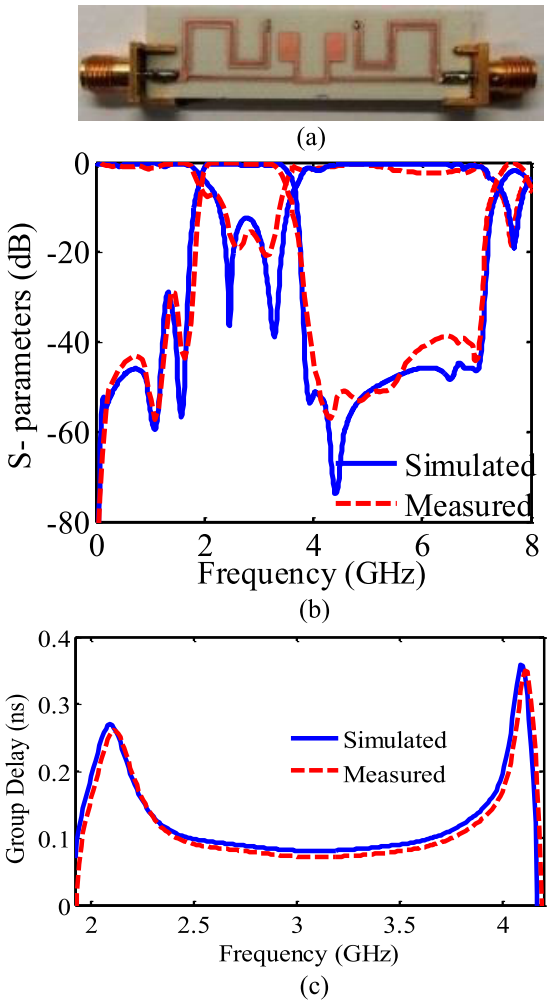

FIGURE 5. (a) Fabricated BPF prototype, (b) Simulated and measured performance of the constant BW BPF (Filter A), (c) Group delay.

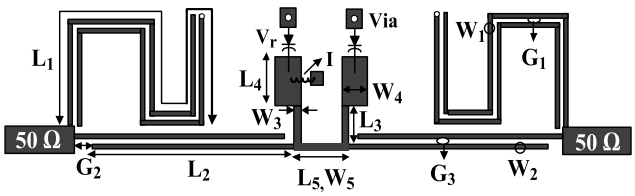

FIGURE 6. Proposed tunable BPF (Filter B), Dimensions: $W_1 = 0.45$, $W_2 = 0.20$, $W_3 = 0.70$, $W_4 = 3.20$, $W_5 = 0.65$, $L_1 = 34.0$, $L_2 = 16.90$, $L_3 = 2.90$, $L_4 = 4.45$, $L_5 = 5.76$, $G_1 = 0.45$, $G_2 = 0.30$, $G_3 = 0.37$ (all units in mm), I = Inductor, Vr = Varactor.

Filter B and are presented in Fig. 6. Filter B was fabricated on Roger 4003C material. The used varactors (SMV2019) have adjustable capacitance range of 0.3-2.2 pF in response to dc bias from 0-20 V. Simple biasing circuits consisting of RF choke inductors (82 nH) to separate the dc from high frequency signal were utilized.

The fabricated prototype of the tunable BPF is shown in Fig. 7(a) along with the measured S-parameter results in Fig. 7(b) and Fig. 7(c). As shown in Fig. 7, the 3-dB FBW

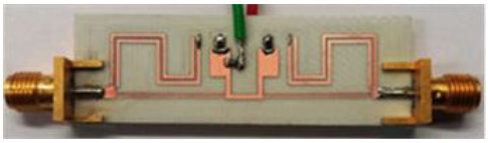

(a)

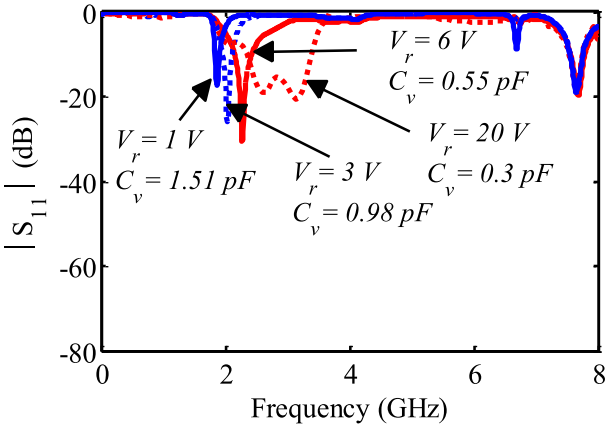

(b)

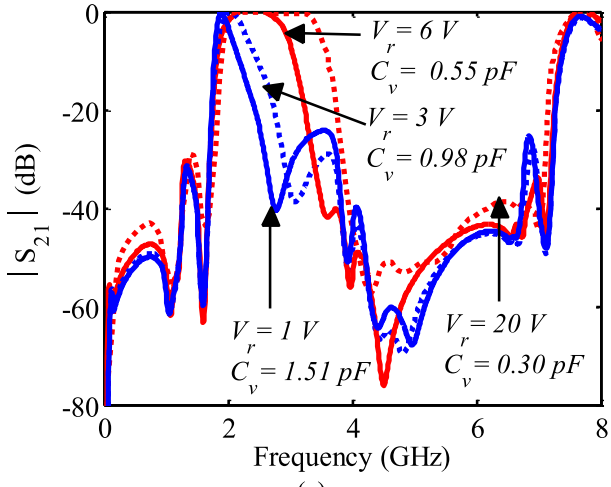

(c)

FIGURE 7. Measured results for filter B, (a) Fabricated tunable BPF prototype, (b) $|S_{11}|$ (c) $|S_{21}|$.

TABLE 3. Comparison with some tunable BPFs.

Ref.	RL (dB)	IL (dB)	3-dB BW tuning ratio	3-dB FBW range (%)	Circuit Size ($\lambda_g \times \lambda_g$)
[22]	> 15	< 1.1	1.28	16.5	0.51×0.51
[23]	> 12	< 1.5	5.00	40.0	0.80×0.70
[25]	> 10	< 2	1.77	20.6	0.62×0.25
[26]	> 10	< 1.4	1.62	21.7	1.03×1.03
[27]	>17	< 0.8	1.79	48.6	0.72×0.50
[28]	> 13	< 2.5	8.65	62.0	0.29×0.22
[29]	> 15	< 4.1	3.54	10.7	1.37×0.22
[31]	> 11	< 1.9	1.91	23.8	0.92×0.55
[32]	> 13	< 1.5	4.30	41.7	0.42×0.14
[33]	> 11	< 2.3	7.70	86.2	0.18×0.12
[34]	> 10	< 2.6	2.31	55.0	1.01×0.46
This work (Filter B)	**> 15**	**< 1.1**	**5.00**	**47.0**	**0.67×0.17**

can be tuned from 12% to 60% corresponding to capacitance increase from 0.30 pF to 1.51 pF. Additionally, the TZ that is close to the higher passband edge shifts from 3.85 GHz to 4.32 GHz to safeguard the filter's sharp skirt. A compact circuit size of 40.1 mm × 9.9 mm ($0.113\lambda_g^2$) is acquired as illustrated in Fig. 7. To emphasize the merits of the proposed tunable BPF, a comparison with other published related works is summarized in Table 3. The proposed filter demonstrates the one of the highest 3-dB tuning ratios (0.27 GHz to 1.80 GHz) and at the same time it covers one of the smallest areas ($0.113\lambda_g^2$) compared to the other filters.

V. CONCLUSION

A novel method for superior selectivity of a stepped-impedance resonator bandpass filter, by employing a pair of open/short-circuited coupled lines, implemented at the input and output stages of the filter, has been demonstrated. As a result, two pairs of symmetrical TZs are added to both sides of the passband, causing high passband selectivity. To demonstrate this method, two high-selectivity wideband BPFs with fixed (Filter A) and tunable bandwidth (Filter B) are presented. Filter A with 60% FBW demonstrates a compact size ($0.113\lambda_g^2$) and presents low IL <0.8 dB, high RL>15 dB throughout the passband, and 40 dB upper stopband rejection. Filter B has been designed to accomplish an extremely wide tuning range for the passband bandwidth by enabling tunable upper band edge transmission zeros. A clear design procedure has been followed and the measured results indicate tuning range variation from 12% to 60% and a 3-dB tuning ratio of 5. The proposed high-performance BPFs demonstrate the following merits that are difficult to present all together: high selectivity and sharp transition bands, compact size, low IL, and clear topology. This $\lambda_g/2$ open/short coupling structure as a basic building block, is expected to be used in combination with other types of filters. These filters will have good perspective for use in new generation wideband communication systems such as ground-based or naval radars.

REFERENCES

[1] K.-D. Xu, D. Li, and Y. Liu, "High-selectivity wideband bandpass filter using simple coupled lines with multiple transmission poles and zeros," *IEEE Microw. Wireless Compon. Lett.*, vol. 29, no. 2, pp. 107–109, Feb. 2019.

[2] C.-J. Chen, "A coupled-line coupling structure for the design of quasi-elliptic bandpass filters," *IEEE Trans. Microw. Theory Techn.*, vol. 66, no. 4, pp. 1921–1925, Apr. 2018.

[3] K. D. Xu, F. Zhang, Y. Liu, and W. Nie, "High selectivity seventh-order wideband bandpass filter using coupled lines and open/shorted stubs," *Electron. Lett.*, vol. 54, no. 4, pp. 223–225, Feb. 2018.

[4] K. D. Xu, F. Zhang, Y. Liu, and Q. H. Liu, "Bandpass filter using three pairs of coupled lines with multiple transmission zeros," *IEEE Microw. Wireless Compon. Lett.*, vol. 28, no. 7, pp. 576–578, Jul. 2018.

[5] R. Gómez-García, L. Yang, J.-M. Muñoz-Ferreras, and D. Psychogiou, "Selectivity-enhancement technique for stepped-impedance-resonator dual-passband filters," *IEEE Microw. Wireless Compon. Lett.*, vol. 29, no. 7, pp. 453–455, Jul. 2019.

[6] W. J. Feng, W. Q. Che, Y. M. Chang, S. Y. Shi, and Q. Xue, "High selectivity fifth-order wideband bandpass filters with multiple transmission zeros based on transversal signal-interaction concepts," *IEEE Trans. Microw. Theory Techn.*, vol. 61, no. 1, pp. 89–97, Jan. 2013.

[7] P. Vryonides, S. Arain, A. Quddious, and S. Nikolaou, "Open-/short-circuited coupled-line structures for the design of high-selectivity bandpass filter," in *Proc. 50th Eur. Microw. Conf. (EuMC)*, Jan. 2021, pp. 128–131.

[8] J. A. G. Malherbe, "Wideband bandpass filter with extremely wide upper stopband," *IEEE Trans. Microw. Theory Techn.*, vol. 66, no. 6, pp. 2822–2827, Jun. 2018.
[9] T. K. Das, S. Chatterjee, S. K. A. Rahim, and T. K. Geok, "Compact high-selectivity wide stopband microstrip cross-coupled bandpass filter with spurline," *IEEE Access*, vol. 10, pp. 69866–69882, 2022.
[10] G. Lin and Y. Dong, "A compact, hybrid SIW filter with controllable transmission zeros and high selectivity," *IEEE Trans. Circuits Syst. II, Exp. Briefs*, vol. 69, no. 4, pp. 2051–2055, Apr. 2022.
[11] W. Zhao, Y. Wu, Y. Yang, and W. Wang, "LTCC bandpass filter chips with controllable transmission zeros and bandwidths using stepped-impedance stubs," *IEEE Trans. Circuits Syst. II, Exp. Briefs*, vol. 69, no. 4, pp. 2071–2075, Apr. 2022.
[12] G. Shen, W. Che, and Q. Xue, "Compact microwave and millimeter-wave bandpass filters using LTCC-based hybrid lumped and distributed resonators," *IEEE Access*, vol. 7, pp. 104797–104809, 2019.
[13] W. M. Fathelbab, "Reconfigurable and tuneable bandpass prototype networks achieving minimal absolute bandwidth variation," *IET Microw., Antennas Propag.*, vol. 9, no. 6, pp. 517–532, Apr. 2015.
[14] M. Yuceer, "A reconfigurable microwave combline filter," *IEEE Trans. Circuits Syst. II, Exp. Briefs*, vol. 63, no. 1, pp. 84–88, Jan. 2016.
[15] A. Zakharov, S. Rozenko, and M. Ilchenko, "Varactor-tuned microstrip bandpass filter with loop hairpin and combline resonators," *IEEE Trans. Circuits Syst. II, Exp. Briefs*, vol. 66, no. 6, pp. 953–957, Jun. 2019.
[16] X. Chen, Y. Wu, Y. Yang, and W. Wang, "Simple coupled-line tunable bandpass filter with wide tuning range," *IEEE Access*, vol. 8, pp. 82286–82293, 2020.
[17] Y.-H. Cho, C. Park, and S.-W. Yun, "0.7–1.0-GHz switchable dual-/single-band tunable bandpass filter using a switchable J-inverter," *IEEE Access*, vol. 9, pp. 16967–16974, 2021.
[18] T. Lim, A. Anand, J. Chen, X. Liu, and Y. Lee, "Design method for tunable planar bandpass filters with single-bias control and wide tunable frequency range," *IEEE Trans. Circuits Syst. II, Exp. Briefs*, vol. 68, no. 1, pp. 221–225, Jan. 2021.
[19] R. Allanic, D. Le Berre, Y. Quere, C. Quendo, D. Chouteau, V. Grimal, D. Valente, and J. Billoue, "A novel synthesis for bandwidth switchable bandpass filters using semi-conductor distributed doped areas," *IEEE Access*, vol. 8, pp. 122599–122609, 2020.
[20] S. Arain, P. Vryonides, A. Quddious, and S. Nikolaou, "Reconfigurable BPF with constant center frequency and wide tuning range of bandwidth," *IEEE Trans. Circuits Syst. II, Exp. Briefs*, vol. 67, no. 8, pp. 1374–1378, Aug. 2020.
[21] J. Xu, "Compact switchable bandpass filter and its application to switchable diplexer design," *IEEE Microw. Wireless Compon. Lett.*, vol. 26, no. 1, pp. 13–15, Jan. 2016.
[22] S. Arain, P. Vryonides, M. A. B. Abbasi, A. Quddious, M. A. Antoniades, and S. Nikolaou, "Reconfigurable bandwidth bandpass filter with enhanced out-of-band rejection using π-section-loaded ring resonator," *IEEE Microw. Wireless Compon. Lett.*, vol. 28, no. 1, pp. 28–30, Jan. 2018.
[23] M. A. Sanchez-Soriano, R. Gomez-Garcia, G. Torregrosa-Penalva, and E. Bronchalo, "Reconfigurable-bandwidth bandpass filter within 10–50%," *IET Microw., Antennas Propag.*, vol. 7, no. 7, pp. 502–509, May 2013.
[24] N. Kumar, S. Narayana, and Y. K. Singh, "Constant absolute bandwidth tunable symmetric and asymmetric bandpass responses based on reconfigurable transmission zeros and bandwidth," *IEEE Trans. Circuits Syst. II, Exp. Briefs*, vol. 69, no. 3, pp. 1014–1018, Mar. 2022.
[25] H.-J. Tsai, N.-W. Chen, and S.-K. Jeng, "Reconfigurable bandpass filter with separately relocatable passband edge," *IEEE Microw. Wireless Compon. Lett.*, vol. 22, no. 11, pp. 559–561, Nov. 2012.
[26] T. Cheng and K.-W. Tam, "A wideband bandpass filter with reconfigurable bandwidth based on cross-shaped resonator," *IEEE Microw. Wireless Compon. Lett.*, vol. 27, no. 10, pp. 909–911, Oct. 2017.
[27] X.-K. Bi, X. Zhang, S.-W. Wong, S.-H. Guo, and T. Yuan, "Synthesis design of Chebyshev wideband band-pass filters with independently reconfigurable lower passband edge," *IEEE Trans. Circuits Syst. II, Exp. Briefs*, vol. 67, no. 12, pp. 2948–2952, Dec. 2020.
[28] M. Tian, Z. Long, L. Feng, L. He, and T. Zhang, "A compact wide-range frequency and bandwidth reconfigurable filter," *IEEE Microw. Wireless Compon. Lett.*, vol. 32, no. 11, pp. 1283–1286, Nov. 2022.
[29] D. Psychogiou and M. Deng, "High-order coaxial bandpass filters with multiple levels of transfer function tunability," *IEEE Microw. Wireless Compon. Lett.*, vol. 30, no. 4, pp. 367–370, Apr. 2020.
[30] H. Zhu and A. Abbosh, "Compact tunable bandpass filter with wide tuning range of centre frequency and bandwidth using coupled lines and short-ended stubs," *IET Microw., Antennas Propag.*, vol. 10, no. 8, pp. 863–870, Jun. 2016.
[31] A. Miller and J. Hong, "Cascaded coupled line filter with reconfigurable bandwidths using LCP multilayer circuit technology," *IEEE Trans. Microw. Theory Techn.*, vol. 60, no. 6, pp. 1577–1586, Jun. 2012.
[32] X. Luo, S. Sun, and R. B. Staszewski, "Tunable bandpass filter with two adjustable transmission poles and compensable coupling," *IEEE Trans. Microw. Theory Techn.*, vol. 62, no. 9, pp. 2003–2013, Sep. 2014.
[33] M. Fan, K. Song, and Y. Fan, "Reconfigurable bandpass filter with wide-range bandwidth and frequency control," *IEEE Trans. Circuits Syst. II, Exp. Briefs*, vol. 68, no. 6, pp. 1758–1762, Jun. 2021.
[34] C. Teng, P. Cheong, S.-K. Ho, K.-W. Tam, and W.-W. Choi, "Design of wideband bandpass filter with simultaneous bandwidth and notch tuning based on dual cross-shaped resonator," *IEEE Access*, vol. 8, pp. 27038–27046, 2020.
[35] S.-C. Tang, P.-C. Chu, J.-T. Kuo, L.-K. Wu, and C.-H. Lin, "Compact microstrip wideband cross-coupled inline bandpass filters with miniaturized stepped-impedance resonators (SIRs)," *IEEE Access*, vol. 10, pp. 21328–21335, 2022.
[36] D. M. Pozar, *Microwave Engineering*, 4th ed. New York, NY, USA: Wiley, 2012.

PHOTOS VRYONIDES (Senior Member, IEEE) received the B.Eng., M.Phil., and Ph.D. degrees in electrical and electronic engineering from the University of Manchester Institute of Science and Technology (UMIST), U.K., in 1998, 1999, and 2002, respectively.

Currently, he is an Associate Professor with Frederick University and a Senior Researcher with the Frederick Research Center (FRC). He is a member of the Antennas and Microwaves Research Group. He has authored or coauthored more than 60 papers in journals and peer-reviewed conferences. His research interests include mixers, LNAs, PAs, broadband amplifiers, millimeter-wave couplers, reconfigurable microwave filters, low-phase noise oscillators, and millimeter-wave MMIC design and components. He is a member of the Technical Chamber of Cyprus. He has been a Cyprus Delegate in the Management Committee of COST IC0803 (RF/Microwave Communication Subsystems for Emerging Technologies) Action and CA18223 (Future Communications with Higher-Symmetric Engineered Artificial Materials). He serves as an Associate Editor for IEEE Access and IEEE Open Journal of Circuits and Systems.

SALMAN ARAIN (Member, IEEE) received the B.E. degree in telecommunication engineering and the M.E. degree in telecommunication engineering and management from the Mehran University of Engineering and Technology, Pakistan, in 2012 and 2014, respectively, and the Ph.D. degree in electrical engineering (RF and microwave reconfigurable circuits) from Frederick University, Nicosia, Cyprus, in 2019, under the Erasmus Mundus INTACT Scholarship Program.

He is currently an Assistant Professor with the NFC Institute of Engineering and Fertilizer Research, Faisalabad, Pakistan. His research interests include reconfigurable/switchable microwave devices, mainly microwave filters and dividers/couplers, the design of optical wireless communication networks, and spread spectrum communication systems. He is a member of IET and the Pakistan Engineering Council (PEC). He received the six-month Mobility Exchange Scholarship under the Erasmus Mundus "Strong Ties" Program to complete the M.Eng. research at Frederick University, from 2013 to 2014. He serves as a Reviewer for various high-quality journal publishers, such as IEEE, IET, Wiley, and Springer, related to the field of microwave circuits and optical networks.

ABDUL QUDDIOUS (Member, IEEE) received the M.Sc. degree in electrical engineering (RF and microwaves) from the Research Institute for Microwave and Millimeter-Wave Studies (RIMMS), NUST, Islamabad, Pakistan, in 2015, and the Ph.D. degree in electrical engineering (focusing on applied electromagnetics) from Frederick University, Nicosia, Cyprus, in 2019. He was a Postdoctoral Researcher with the KIOS Research and Innovation Center of Excellence, University of Cyprus, in 2022. Currently, he is a Senior Researcher with the Chair of Radio Frequency and Photonics Engineering, Dresden University of Technology. His research interests include passive and active antennas, RF electronics, wireless power transfer, RFIDs, and biomedical wireless sensors. He has earned accolades, including the Erasmus Mundus INTACT Doctoral Scholarship, in 2016, and the Gold Plaque for Academic Excellence from Frederick University, in 2019.

DIMITRA PSYCHOGIOU (Senior Member, IEEE) received the Dipl.-Eng. degree in electrical and computer engineering from the University of Patras, Patras, Greece, in 2008, and the Ph.D. degree in electrical engineering from the Swiss Federal Institute of Technology (ETH), Zürich, Switzerland, in 2013.

She is currently a Professor of electrical and electronic engineering with University College Cork (UCC); the Head of the Advanced RF Technology Group, Tyndall National Institute, Cork, Ireland; and an SFI Research Professor. Prior to joining UCC, she was a Senior Research Scientist with Purdue University, West Lafayette, IN, USA, and an Assistant Professor with the University of Colorado at Boulder, Boulder, CO, USA. Her current research interests include RF design and characterization of reconfigurable microwave and millimeter-wave passive components and antennas, RF MEMS, acoustic wave resonator-based filters, tunable filter synthesis, and additive manufacturing techniques for 3D antenna systems. She is a Senior Member of URSI and a member of the IEEE MTT-S Filters and Passive Components (MTT-5) and the Microwave Control Materials and Devices (MTT-13) Committees. Furthermore, she serves on the Technical Review Board for various IEEE and EuMA conferences and journals. Her research has been presented in more than 200 IEEE publications and has received the 2021 Research Professorship Award from the Science Foundation Ireland, the 2021 Roberto Sorrentino Prize from the European Microwave Association (EuMA), the 2020 CAREER Award from the National Science Foundation (NSF), USA, the 2020 URSI Young Scientist Award, and the Junior Faculty Outstanding Research Award from UC Boulder. She serves as the Chair of MMT-13 and the Secretary of USNC-URSI Commission D. She is also an Associate Editor of IEEE Microwave and Wireless Components Letters and *International Journal of Microwave and Wireless Technologies*. Previously, she was an Associate Editor of *IET Microwaves, Antennas and Propagation* journal.

SYMEON NIKOLAOU (Senior Member, IEEE) received the B.S. degree in electrical and computer engineering from the National Technical University of Athens, in 2003, and the M.S. and Ph.D. degrees in electrical and computer engineering from the Georgia Institute of Technology, in 2005 and 2007, respectively.

Currently, he is a Professor with Frederick University, Cyprus, and a Senior Researcher with the Frederick Research Center. His research interests include the design of smart antennas, RFIDs/sensors, wearable and implantable antennas, and reconfigurable components for wireless transceivers. He is a member of the Technical Chamber of Cyprus and has been Cyprus' Delegate in the Management Committee of COST IC0603 (ASSIST—Antenna Systems and Sensors for Information Society Technology) Action, and the substitute Delegate for Cyprus' Substitute Delegate in the Management Committee of COST IC1102 (VISTA Action on Versatile, Integrated, and Signal-Aware Technologies for Antennas) Action. He is currently serving as Cyprus' Delegate in the Management Committee of COST MiMED 1301 Accelerating the Technological, Clinical, and Commercialization Progress in the area of medical microwave imaging. He serves as a Reviewer for IEEE Transactions on Antennas and Propagation, IEEE Transactions on Advanced Packaging, IEEE Antennas and Wireless Propagation Letters, and *IET Letters*. He is currently an Associate Editor of *IET Microwaves Antennas and Propagation* and Open Access *International Journal on Antennas and Propagation* (IJAP).